CHAPTER 4–WIND AND TURBULENT TRANSFER

4.1 AIR FLOW OVER A RIGID SURFACE: SOME DEFINITIONS AND CONCEPTS

In considering the flow of air over the earth's surface, we can envision a very thin layer of air immediately above the surface where the transfer processes are controlled primarily by molecular diffusion. This layer is called the **laminar sublayer**. The laminar sublayer may be only a few millimeters thick and may, sometimes, be even thinner, especially under windy conditions. Above the laminar sublayer is the **turbulent surface layer** (or simply the **surface layer**) which extends up to about 50–100 m and is dominated by strong mixing or eddying motion. The wind structure in this layer is primarily determined by the nature of the underlying surface and the vertical gradient of air temperature. The effect of the earth's rotation, the Coriolis force, is small and may be neglected as the frictional effects of the surface dominate. The **planetary boundary layer**, which envelops the surface layer and extends to about 1 km above the surface, is a zone of transition from the disturbed flow near the surface to the frictionless or smooth flow of the free atmosphere (Sutton, 1953).

In the surface layer, the layer of greatest interest in micrometeorology, the air motion is highly irregular and is characterized by fluctuations, vortices, or eddies. Under lapse conditions, for example, small and relatively rapid and irregular fluctuations in air motion appear to be superimposed on larger and much slower irregular fluctuations. The small fluctuations associated with high frequencies are primarily due to **mechanical turbulence** generated by the frictional effects of the surface. The larger fluctuations associated with low frequencies are the result of **thermal turbulence** arising from the effects of buoyancy.

It is important to note that, even though the air flow in the surface layer is not regular, the overall behavior of average properties such as wind speed, air temperature, humidity, and carbon dioxide concentration can be examined systematically on a statistical basis. For this purpose averaging periods of about 30 min to 1 h are considered adequate.

4.2 WIND SPEED PROFILE AND MOMENTUM EXCHANGE

Knowledge of the shape of the wind profile (variation of wind speed with height) is necessary for, at least, two reasons. From the profile description, it is possible to estimate the effectiveness of vertical exchange processes. With the knowledge of wind speed at a fixed or reference level, it is also possible to estimate wind speed at other levels for various applications.

When a fluid flows along a rigid surface, fluid particles close to the surface are slowed down because of the drag exerted on the flow by the underlying surface. The drag or flow retardation forces cause marked variation in mean horizontal wind speed with height (Fig. 4.1). Momentum is defined as the product of mass and velocity. Employing an analogy to heat transfer, which is directed from a warmer to a cooler location, an examination of Fig. 4.1. leads to the conclusion that horizontal momentum (mass × horizontal wind speed) is transferred from higher to lower elevations or from airflow to the underlying surface.

The total drag force per unit of surface area is called the **shearing stress** τ. The dimensions of shearing stress are the same as those of momentum per unit area per unit time (i.e., momentum flux). Thom (1975) suggests that the wind drag on a surface is simply a manifestation of the continuous downward transport of horizontal momentum from the airflow to the surface. The magnitude of the momentum flux is indicative of the effectiveness of turbulence in exchanging water vapor, sensible heat, carbon dioxide, and other entities between the surface and the atmosphere.

Typical shapes of mean wind profiles are given in Figs. 4.1 and 4.2. Under conditions of neutral atmospheric stability, the mean wind speed profile over an open, level and relatively smooth site can be described as a logarithmic function of elevation (Fig. 4.1):

$$U(z) = \frac{u_*}{k} \ln \frac{z}{z_0} \tag{4.1}$$

where $U(z)$ is the mean wind speed at height z, k is von Karman's constant (with a value of about 0.4), u_* is the friction velocity, and z_0 is the roughness parameter.

A surface is said to be "rough" if it is corrugated or covered with protuberances, usually referred to as **roughness elements**. For mean wind speed profiles over rough surfaces,* such as crop canopies, a zero plane displacement d is introduced (see Fig. 4.2) and (4.1) transforms into

$$U(z) = \frac{u_*}{k} \ln \frac{z - d}{z_0} \tag{4.2}$$

* Some recent observations (e.g., Garratt, 1980) over very rough surfaces, such as forests, indicate that the logarithmic law may not be completely applicable, particularly very close to the top of the roughness elements.

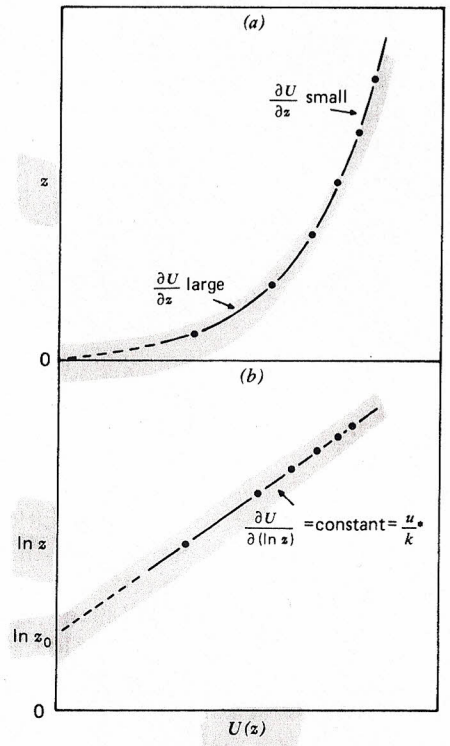

Fig. 4.1 Typical wind profile over an open, level (relatively smooth) site: (*a*) plotted linearly against height z; (*b*) plotted against the logarithm of z. From A. S. Thom, 1975, Momentum, mass and heat exchange of plant communities, In *Vegetation and the Atmosphere,* Vol. 1, *Principles,* J. L. Monteith (ed.). Copyright by Academic Press, Inc. (London), Ltd.

Equations 4.1 or 4.2 are often referred to as the logarithmic law of wind speed profiles.

The **friction velocity** u_* is given by

$$u_* = \left(\frac{\tau}{\rho_a}\right)^{1/2} \tag{4.3}$$

where τ is the shearing stress and ρ_a is the air density. u_* represents a characteristic velocity of the flow and relates to the effectiveness of turbulent exchange over the surface.

The **roughness length** or **roughness parameter** z_0 is a measure of the aerodynamic roughness of the surface over which the wind speed profile is measured. z_0 is determined by extrapolating measured $U(z)$ and ln z to the point where $U = 0$ (see Fig. 4.1). In the case of crops and other rough surfaces ln z is replaced by ln$(z - d)$ as shown in Fig. 4.2.

The roughness parameter for crops is about an order of magnitude smaller than the crop height h. Szeicz et al. (1969) summarized a number of studies and empirically related z_0 to crop height h by

$$\log_{10} z_0 = 0.997 \log_{10} h - 0.883 \tag{4.4}$$

where z_0 and h are in meters.

The **zero plane displacement** d can be considered to indicate the mean level at which momentum is absorbed by the individual elements of the plant community, that is, the level of action of the bulk aerodynamic drag on the community (Thom, 1971, 1975). In general, d/h ranges between 0.5 and 0.8. Figure 4.2*b* shows a graphical procedure used to determine d and z_0 from measured wind speed profiles under nearly neutral conditions. By trial and error, one finds a value of d such that a plot of U (on the linear scale) versus

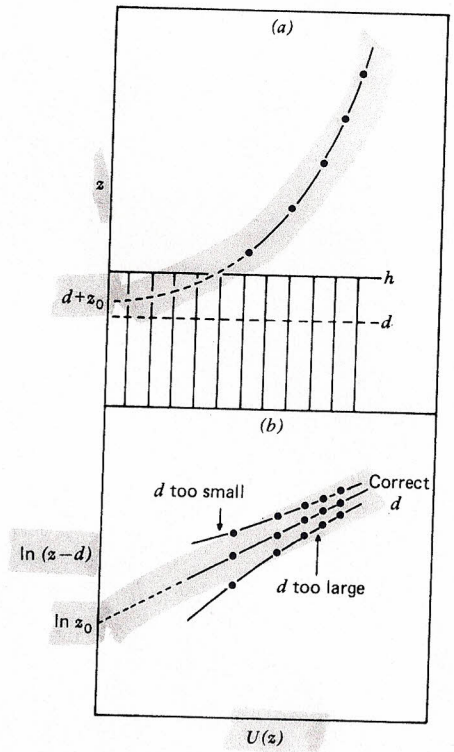

Fig. 4.2 Typical wind profile over uniform level vegetation of height h: (*a*) plotted linearly against z; (*b*) plotted against the logarithm of distance above the zero plane displacement level. From A. S. Thom, 1975, Momentum, mass and heat exchange of plant communities, In *Vegetation and the Atmosphere,* Vol. 1, *Principles,* J. L. Monteith (ed.). Copyright by Academic Press, Inc. (London), Ltd.

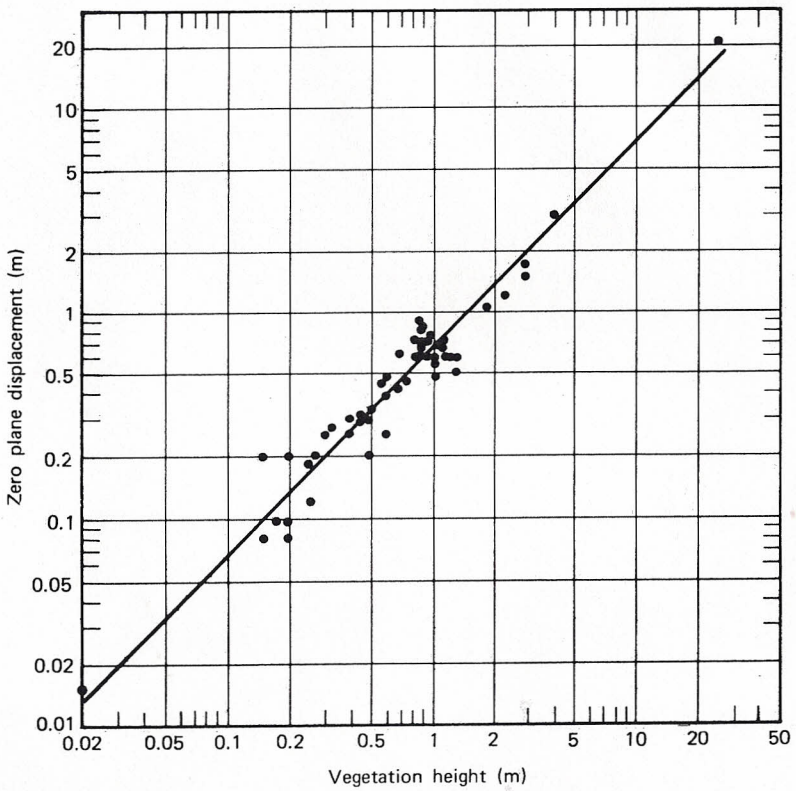

Fig. 4.3 Relationship between zero plane displacement d and vegetation height h for different forms of vegetation and bare ridged soil (after Stanhill, 1969).

$z - d$ (on the log scale) becomes a straight line. The intercept on the $z - d$ axis gives z_0, and the slope of this straight line is u_*/k.

Stanhill (1969) fitted an expression giving zero plane displacement d as a function of crop height h for a wide range of crops (Fig. 4.3):

$$\log_{10} d = 0.979 \log_{10} h - 0.154 \qquad (4.5)$$

where h and d are in meters.

The ratios d/h and z_0/h depend on the spacing of roughness elements and on the ratio of the accumulated area of each element to a unit area of the underlying surface (Monteith, 1973). The problem of accurately estimating z_0 and d is increased by the fact that crops, tall or short, adjust to the mechanical force of the wind. Sometimes bending occurs, as in small grains. Some crops become "streamlined" by the force of the wind (see a review by Makkink and van Heemst, 1970, for further details).

From the above discussion it is clear that, with knowledge of z_0 and d,

the complete wind profile above the canopy can be constructed from the value of U at a fixed or reference level

$$\frac{U_2}{U_1} = \frac{\ln(z_2 - d) - \ln z_0}{\ln(z_1 - d) - \ln z_0} \qquad (4.6)$$

where U_1 and U_2 are the mean wind speeds at elevation z_1 and z_2, respectively (here z_1 can be considered the reference level). It is important to note that validity of the logarithmic wind profile equations (4.1 or 4.2) is subject to two major assumptions: (1) the existence of neutral atmospheric stability and (2) the availability of adequate "fetch" or upwind distance of uniform crop cover or roughness. Stability conditions and fetch requirements are discussed in the following sections. Also note that to obtain adequate mean wind speed values for use in (4.1), (4.2), and (4.6) averaging should be done over a period of at least 15 min and preferably over 30–60 min.

4.3 INTERNAL BOUNDARY LAYER AND FETCH REQUIREMENTS

Each field or surface feature of varying roughness or height affects the airstream passing over it. In moving downwind after a change in surface roughness is encountered at the "leading edge", air begins to adjust to the new surface boundary conditions (see Fig. 4.4). The layer of air downwind of the leading edge, affected by the new underlying surface, is called the **internal boundary layer**.* Thickness δ of the internal boundary layer increases with fetch or distance downwind of the leading edge. Wind tunnel experiments and other micrometeorological studies suggest that only the lowest 10% of the internal boundary layer is "fully adjusted", that is, in complete equilib-

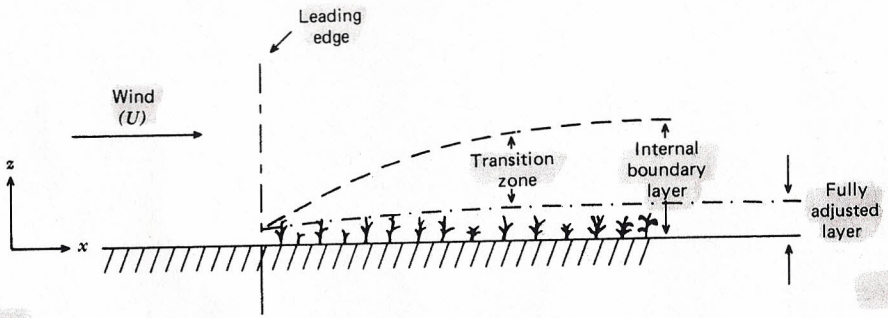

Fig. 4.4 The development of an internal boundary layer as air flows from a smooth to a rougher vegetation surface (adapted from Oke, 1978).

* In the discussion presented here, we have concentrated on the leading edge effect on wind flow resulting from a change in surface roughness. Similar concepts can be applied to leading edge effects resulting from changes in surface temperature or humidity.

rium with the new boundary conditions. The thickness of this fully adjusted layer δ_1, measured above the zero plane displacement, can be approximated according to Munro and Oke (1975) by

$$\delta_1(x) = 0.1x^{4/5}z_0^{1/5} \tag{4.7}$$

where x is the distance downwind from the leading edge and z_0 is the roughness parameter of the new underlying surface.

The air flow is fully equilibrated with the new surface to the depth $\delta_1(x)$. Therefore, a logarithmic wind profile characteristic of the underlying surface should develop to that depth. The flux of momentum should be independent of height in the fully adjusted layer. One may derive, using (4.7), the height to fetch ratio that determines the limit below which sensors must be placed to properly represent conditions in the fully adjusted layer. Appropriate values of surface roughness z_0 must be applied, however. Equation 4.7 yields a height to fetch ratio of about 1:50 for agricultural crops. For safety sake, a height to fetch ratio of 1:100 is usually considered adequate for studies made over agricultural crop surfaces. This means that in a field with uniform crop cover and upwind fetch of 200 m a layer about 2 m deep will develop in which the logarithmic wind profile relationships prevail. In this layer flux is almost independent of height.

4.4 ATMOSPHERIC STABILITY

The concept of atmospheric thermal stability was inroduced in Chapter 3. Turbulence is enhanced by buoyancy forces under unstable conditions and is suppressed under stable conditions. The effects of thermal stability on the shape of the wind speed profile and on the turbulent exchange rate (discussed in the next section) are generally expressed in terms of two nondimensional parameters: the **Richardson number** (Ri) and the **Monin–Obukhov parameter** z/L. The Richardson number (often called the gradient Richardson number) is given by

$$\mathrm{Ri} = \frac{g(\partial\theta/\partial z)}{T(\partial U/\partial z)^2} \tag{4.8}$$

where g is the acceleration due to gravity, $\partial\theta/\partial z$ and $\partial U/\partial z$ are the vertical gradients of mean potential temperature and mean horizontal wind speed, and T is the mean absolute temperature (degrees Kelvin). Ri can be interpreted as a parameter describing the relative importance of buoyancy and mechanical forces, that is, the relative importance of free versus forced convection. The sign of Ri is determined by the gradient of potential temperature which is negative in lapse (or unstable), and positive under inversion (or stable) conditions. Ri approaching zero implies near neutral conditions. For application in the first 1–2 m above ground, the Richardson number may be calculated with $\partial T/\partial z$ substituted for $\partial\theta/\partial z$ in (4.8).

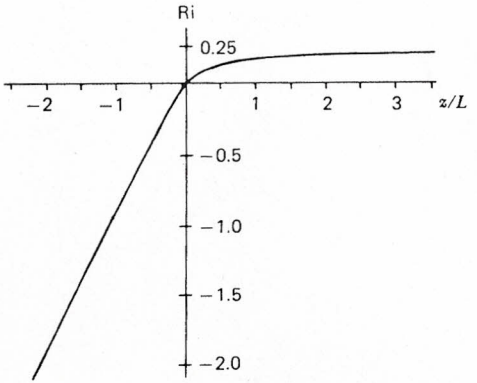

Fig. 4.5 Relationship between Richardson number Ri and the Monin–Obukhov stability parameter z/L (adapted from Businger et al., 1971).

The Monin–Obukhov stability parameter (z/L) given by

$$z/L = \frac{kzgH}{\rho_a C_p T u_*^3} \tag{4.9}$$

is derived as the ratio of buoyant production to mechanical production of turbulence, where H is the sensible heat flux* and C_p is the specific heat of air at constant pressure (for further details, see Lumley and Panofsky, 1964). Measurements of sensible heat flux H and friction velocity u_* are needed to evaluate this parameter. Theoretically, z/L is considered a more precise indicator of thermal stability than Ri. Ri, however, requires measurement of wind speed and air temperature gradients only, and is easier to evaluate in practice. A typical relationship between Ri and z/L observed in the surface layer is given in Fig. 4.5 (adapted from Businger et al., 1971).

Moist air is less dense than dry air. To account for the effect of moisture on buoyancy a virtual temperature, T_v (°K) is defined by

$$T_v = T(1 + 0.6q) \tag{4.10}$$

where T is the absolute temperature (°K) and q is the specific humidity. The use of virtual temperature (T_v) in lieu of the actual temperature makes it possible to apply the ideal gas law for moist air in the same way as for dry air. Therefore, when buoyancy forces are involved, gradients of T_v rather that T should be considered. For further details the reader is referred to Lumley and Panofsky (1964), Webb (1965), Plate (1971), and Busch (1973).

* Note that the sign convention employed in this book is such that all fluxes toward the ground surface are positive and all away from the surface are negative.

4.5 FLUX PROFILE RELATIONSHIPS

In aerodynamic theory, the transfer of momentum, sensible heat, water vapor, or any other entity may be estimated by analogous equations

$$\text{momentum flux:} \quad \tau = \rho_a K_m \frac{\partial U}{\partial z} \tag{4.11}$$

$$\text{sensible heat flux:} \quad H = \rho_a C_p K_h \frac{\partial \theta}{\partial z} \tag{4.12}$$

$$\text{water vapor flux:} \quad E = \frac{(M_w/M_a)}{P} \rho_a K_w \frac{\partial e_a}{\partial z} \tag{4.13}$$

where K_m, K_h, and K_w are the turbulent exchange coefficients for momentum, sensible heat, and water vapor, respectively; ρ_a is the air density; C_p is the specific heat at constant pressure; P is the atmospheric pressure; $\partial U/\partial z$, $\partial\theta/\partial z$, and $\partial e_a/\partial z$ are the vertical gradients of mean wind speed, potential temperature, and vapor pressure, respectively; M_w and M_a are the molecular weights of water vapor and air.

If these exchange coefficients are assumed to be identical, then a knowledge of any one in conjunction with the appropriate gradient measurements permits the estimation of any and all of the fluxes. This assumption of identity of exchange coefficients is called *Reynolds analogy*.

Observations suggest that the assumption of identity in exchange coefficients is valid only when the atmosphere is in a condition of nearly neutral stability. Such conditions normally prevail for only limited periods of the day. The effects of atmospheric stability on the relationship between exchange coefficients under nonneutral conditions has been determined experimentally in several micrometeorological investigations. Some recent findings are summarized below

$$\left.\begin{array}{lll}
\text{unstable conditions:} & \dfrac{K_h}{K_m} \approx \dfrac{K_w}{K_m} = (1 - 16\ \mathrm{Ri})^{0.25} & \text{(Dyer and Hicks, 1970)} \\
& \dfrac{K_w}{K_m} = 1.13\ (1 - 60\ \mathrm{Ri})^{0.074} & \text{(Pruitt et al., 1973)} \\
\text{stable conditions:} & \dfrac{K_h}{K_m} \approx \dfrac{K_w}{K_m} \approx 1 & \text{(Webb, 1970)} \\
& \dfrac{K_w}{K_m} = 1.13\ (1 + 95\ \mathrm{Ri})^{-0.11} & \text{(Pruitt et al., 1973)}
\end{array}\right\} \tag{4.14}$$

As discussed in Section 4.2, the logarithmic wind profile equations are valid only in neutral conditions. When nonneutral conditions exist, the shape of the wind profile deviates significantly from the logarithmic ideal (Fig. 4.6). The change in shape of the wind profile due to thermal stability effects

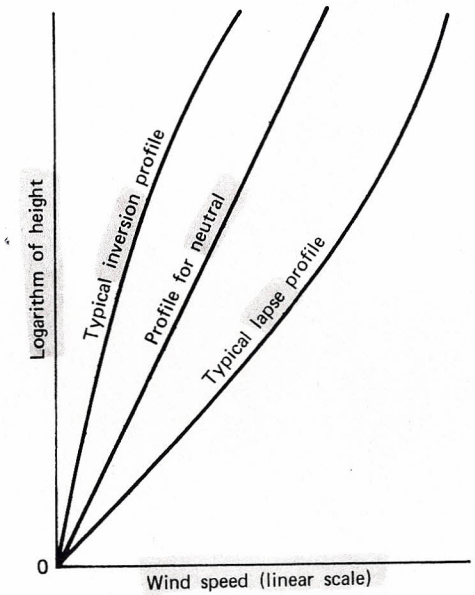

Fig. 4.6 Shape of the wind profile as a function of atmospheric stability (after Sutton, 1953).

is accounted for by introducing a dimensionless stability function ϕ_m (Monin and Obukhov, 1954) given by

$$\frac{\partial U}{\partial z} = \frac{u_*}{kz} \phi_m \tag{4.15}$$

where ϕ_m is generally expressed as a function of Richardson number Ri or z/L (L the Monin–Obukhov stability parameter). [Use $(z - d)$ instead of z in (4.15) for rough surfaces.] Note that for neutral conditions ϕ_m is equal to 1 and (4.15) converts into the logarithmic wind profile equation (4.1). There have been many efforts to precisely define the functional relationships between ϕ_m and Ri (or z/L) in stable and unstable conditions (see Holzman, 1943; Panofsky, 1963; Lumley and Panofsky, 1964; Dyer and Hicks, 1970; Webb, 1970; Oke, 1970; Swinbank, 1964, 1968; Businger et al., 1971; Pruitt et al., 1973). Some recent results are given below

$$\left.\begin{array}{ll}
\text{unstable conditions:} & \phi_m = (1 - 16\ \mathrm{Ri})^{-0.25} \quad \text{(Dyer and Hicks, 1970)} \\
& \phi_m = (1 - 16\ \mathrm{Ri})^{-1/3} \quad \text{(Pruitt et al., 1973)} \\
\text{stable conditions:} & \phi_m = (1 - 5.2\ \mathrm{Ri})^{-1} \quad \text{(Webb, 1970)} \\
& \phi_m = (1 + 16\ \mathrm{Ri})^{1/3} \quad \text{(Pruitt et al., 1973)}
\end{array}\right\} \tag{4.16}$$

For further detailed evaluation of these relationships, the reader is referred to Dyer (1974), Wieringa (1980), and Francey and Garratt (1981).

Employing (4.11) and (4.15), the equations for sensible heat (4.12) and water vapor flux (4.13) can be rewritten as

$$\text{sensible heat flux} = H = \rho_a C_p k^2 z^2 \left(\frac{\partial U}{\partial z}\right)\left(\frac{\partial \theta}{\partial z}\right)\left(\frac{K_h}{K_m}\phi_m^{-2}\right) \tag{4.17}$$

$$\text{water vapor flux} = E = \frac{(M_w/M_a)}{P}\rho_a k^2 z^2 \left(\frac{\partial U}{\partial z}\right)\left(\frac{\partial e_a}{\partial z}\right)\left(\frac{K_w}{K_m}\phi_m^{-2}\right) \tag{4.18}$$

Therefore, with knowledge of the appropriate gradients ($\partial U/\partial z$, $\partial\theta/\partial z$, $\partial e_a/\partial z$), in conjunction with the stability corrections [(4.14) and (4.16)], the fluxes of sensible heat, water vapor, or any other entity may be estimated from the flux gradient relationships described above.*

4.6 EDDY CORRELATION TECHNIQUE FOR ESTIMATING ENERGY AND MASS FLUXES

In fully turbulent flow the mean vertical flux F of an entity s per unit mass of the fluid is given by

$$F = \overline{\rho_a w s} \tag{4.19}$$

where ρ_a is the air density, w is the vertical velocity, and the overbar denotes the average value during a time period of suitable length.

In the surface layer, as discussed in Section 4.1, all atmospheric entities exhibit short-period fluctuations about their mean value (see Fig. 4.7 for an example). Therefore, the instantaneous values of w, s, and ρ_a in (4.19) can be expressed by

$$w = \bar{w} + w', \qquad s = \bar{s} + s', \qquad \text{and} \qquad \rho_a = \bar{\rho}_a + \rho_a' \tag{4.20}$$

where the prime symbol denotes an instantaneous departure from the mean. These expressions can be substituted into (4.19) and, if we neglect fluctuations in density, the mean vertical flux F reduces† to

$$F = \bar{\rho}_a \overline{ws} + \bar{\rho}_a \overline{w's'} \tag{4.21}$$

or by writing ρ_a for $\bar{\rho}_a$

$$F = \rho_a \overline{ws} + \rho_a \overline{w's'} \tag{4.22}$$

* Note that for proper applications of the stability correction models described in (4.14) and (4.16) appropriate values of k (as suggested in the respective reports) should be used: for the Dyer and Hicks (1970) and Webb (1970) models, use $k = 0.4$ but for the Pruitt et al. (1973) model, use $k = 0.42$. For rough surfaces, use $(z - d)^2$ instead of z^2 in (4.17) and (4.18).

† Note that the following rules (the Reynolds rules of averaging) apply: $x = \bar{x} + x'$; $y = \bar{y} + y'$; $\bar{x}' = \bar{y}' = 0$; $\overline{x + y} = \bar{x} + \bar{y}$; $\overline{x'y'} \neq 0$.

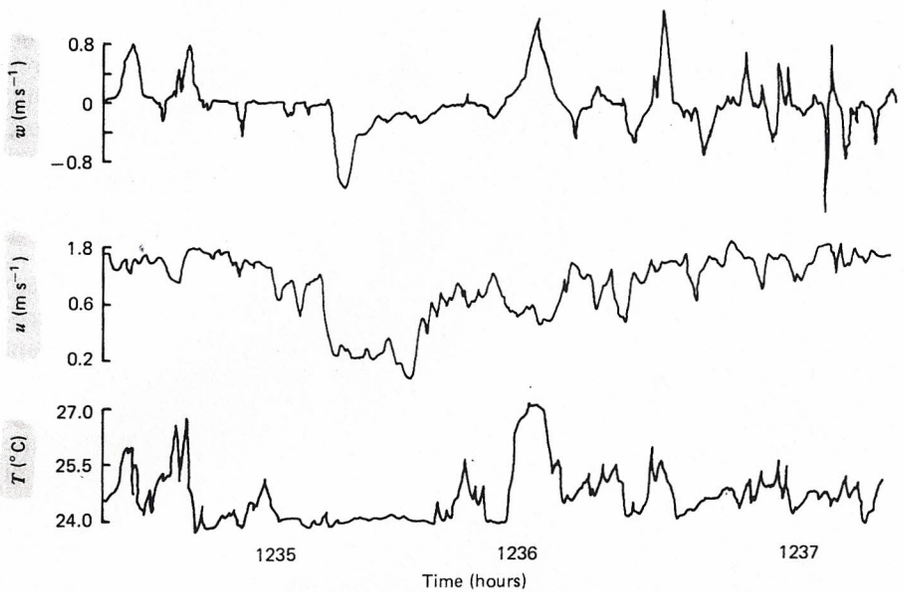

Fig. 4.7 Simultaneous recordings of signals from fast response sensors of vertical wind speed w, horizontal wind speed u and air temperature T above a corn crop. Reprinted from *Physiological Aspects of Crop Yield,* Chapter 6 by Edgar Lemon, page 132, 1969, by permission of the American Society of Agronomy and Crop Science Society of America.

The first term on the right-hand side of (4.22) represents flux due to the mean vertical flow or mass transfer. The second term represents flux due to eddying motion or eddy flux. The mass transfer term may arise from a convergence or divergence of air due to sloping surface. For a sufficiently long period of time over horizontally uniform terrain the total quantity of ascending air is approximately equal to the quantity descending and the mean value of the vertical velocity will be negligible. Therefore, (4.22) reduces to

$$F \approx \rho_a \overline{w's'} \tag{4.23}$$

Based on the above equation, the fluxes of momentum, sensible heat, and water vapor can be expressed as

$$\text{momentum flux:} \quad \tau = -\rho_a \overline{u'w'} \tag{4.24}$$

$$\text{sensible heat flux:} \quad H = -\rho_a C_p \overline{w'T'} \tag{4.25}$$

$$\text{water vapor flux:} \quad E = -\frac{\epsilon}{P}\rho_a \overline{w'e_a'} \tag{4.26}$$

where u', T', and e_a' are instantaneous departures from the mean horizontal

velocity, air temperature, and vapor pressure; ϵ is the ratio of molecular weights of water vapor and air $= M_w/M_a$ and P is the atmospheric pressure.

Some recent analyses (e.g., Webb et al., 1980; Webb, 1982) indicate that atmospheric turbulent fluxes of minor constituents such as water vapor and CO_2 may be influenced by density variations due to simultaneous transfers of sensible heat and water vapor (the density effect may cause a very small but non zero mean vertical air speed). For further details on these effects the reader is referred to the original publications.

The eddy correlation technique, when properly applied, provides reasonably accurate estimates of fluxes more directly than do the other micrometeorological methods. Over rough surfaces, for example, the turbulent exchange coefficients are large and hence vertical gradients of temperature and humidity are exceedingly small. Correspondingly, vertical velocity fluctuations are quite large. Therefore, as Kanemasu et al. (1979) point out the eddy correlation technique should be more accurate than those methods that rely on measurement of vertical gradients. Instrumentation for measurement of turbulent fluctuations has been under development for a number of years. These instruments include hot wire anemometers, sonic anemometers, drag anemometers and propeller anemometers for the measurement of velocity fluctuations, fine wire thermocouples (dry and wet bulb) or sensitive thermistors to sense temperature fluctuations (see Chapter 3), and hygrometers (infrared and Lyman-alpha) to sense humidity fluctuations (see Chapter 5).

In the application of the eddy correlation technique, two points require particular attention. First, instruments must be so sensitive as to be able to detect simultaneous changes (fluctuations) in quantities such as velocity, temperature, and humidity caused by the rapid passage of different eddies. The frequency of these fluctuations increases as the surface is approached. The less sensitive the sensors, the higher above the surface they must stand and thus the greater the likelihood that they will be outside the fully adjusted layer. Second, a capability to quickly record and process the large quantities of data produced by these sensors is required. With the continuing improvements in instrumentation, data acquisition, and computing systems, the use of the eddy correlation technique for estimating energy and mass fluxes in the atmospheric surface layer is becoming more and more practical.

4.7 WIND SPEED WITHIN CROP CANOPIES

In previous sections, we have discussed the difficulties involved in accurately describing mean wind profile relationships above plant canopies. Wind speed relationships within canopies are still more difficult to establish. A good example of the complexity of the wind structure in canopies is found in Fig. 4.8 due to Allen (1968) showing the shape of a typical wind profile in a Japanese larch tree plantation in upper New York State. Campbell (1977) considers that the within-canopy flow regime is divided into three layers

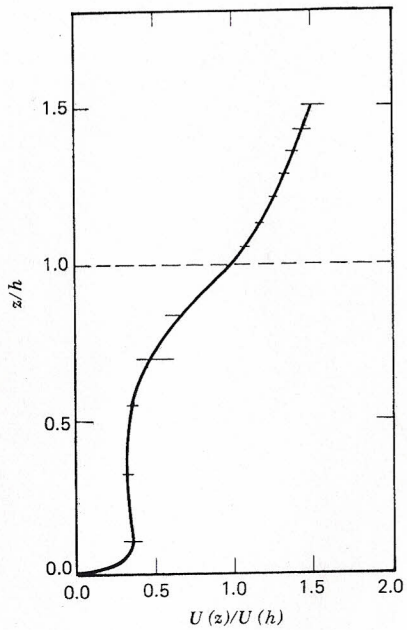

Fig. 4.8 Average normalized wind speed above and within a Japanese larch plantation, mid-November, near Ithaca, New York (after Allen, 1968).

which are evident in Fig. 4.8:

1. The top layer ($d < z < h$) is the layer that exerts most of the drag on the wind above the crop. The wind in this layer decreases exponentially with distance downward from the canopy top and has the same direction as the mean wind above the canopy.
2. The second layer (about $0.1\ h < z < d$) is comprised mainly of the stem space of the crop. There the wind may be quite unrelated, in both speed and direction, to the wind above the canopy.
3. The wind profile in the third layer ($z < 0.1\ h$) is similar in shape to the above canopy logarithmic profile. The profile in this layer is influenced, however, by the soil surface roughness instead of by the crop roughness.

4.8 DAILY WIND PATTERNS

Wind speed increases with elevation above the ground surface. Under fairly constant weather conditions a diurnal wave of wind speed can be detected at levels of measurements near the ground. A typical pattern is given in Fig. 4.9 for wind at a number of levels aboveground. Nighttime situations are normally calm, and peak wind speeds usually occur near noon.

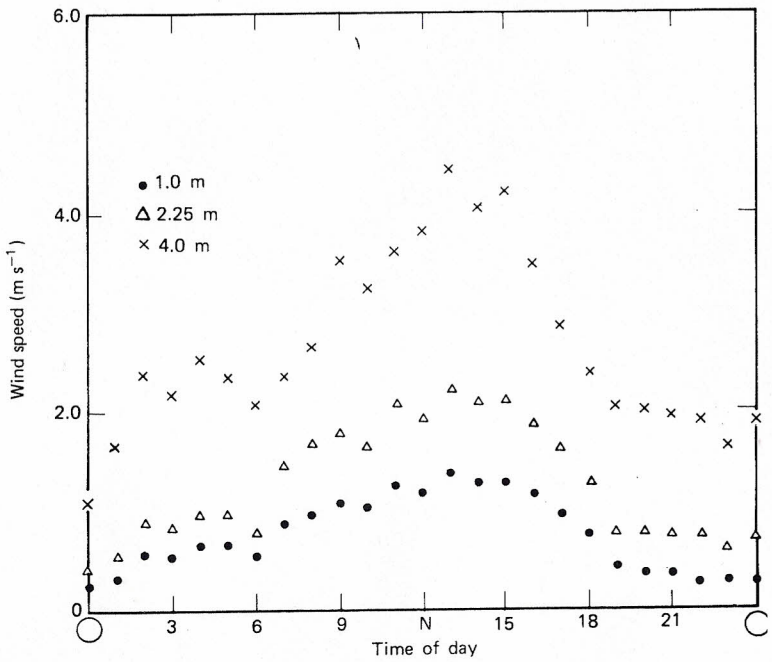

Fig. 4.9 Daily course of wind speed over 50 cm tall soybeans, early July, at Mead, Nebraska.

This normal condition is especially apparent in climatological summaries where the diurnal wind speed patterns over many days are summarized and the means are calculated. In regions of strong frontal activity or where convective storms are common, however, the actual daily patterns of wind speed are much more variable.

4.9 SEASONAL PATTERNS OF WIND DIRECTION AND SPEED

It is beyond the scope of this work to discuss the many large-scale and local seasonal patterns of winds that prevail in differing climatic regions of the world. It is important, however, to recognize that there do exist such recurring patterns and that these can be identified through climatological surveys and can be predicted with some degree of certainty by the methods of statistical climatology. Our own work in characterizing the wind regime in the central Great Plains may serve as a useful example.

The distribution of wind speed and direction at a given location is often presented in the form of a "wind rose" which is a polar plot of the frequency of wind flow as a function of wind direction (Slade, 1968). Some typical wind roses for Grand Island, Nebraska, are shown in Fig. 4.10. The data represent

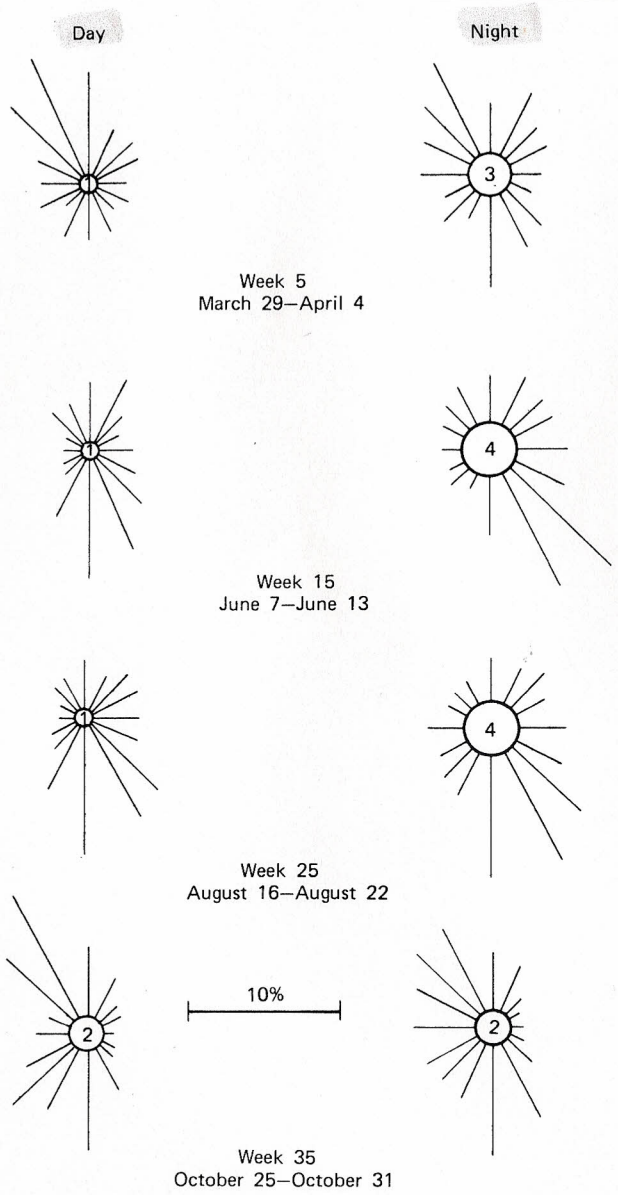

Fig. 4.10 Percentage frequencies of wind direction for day and night during 4 weeks of the growing season at Grand Island, Nebraska. Percent of calm hours indicated in center circle (after Rosenberg, 1965).

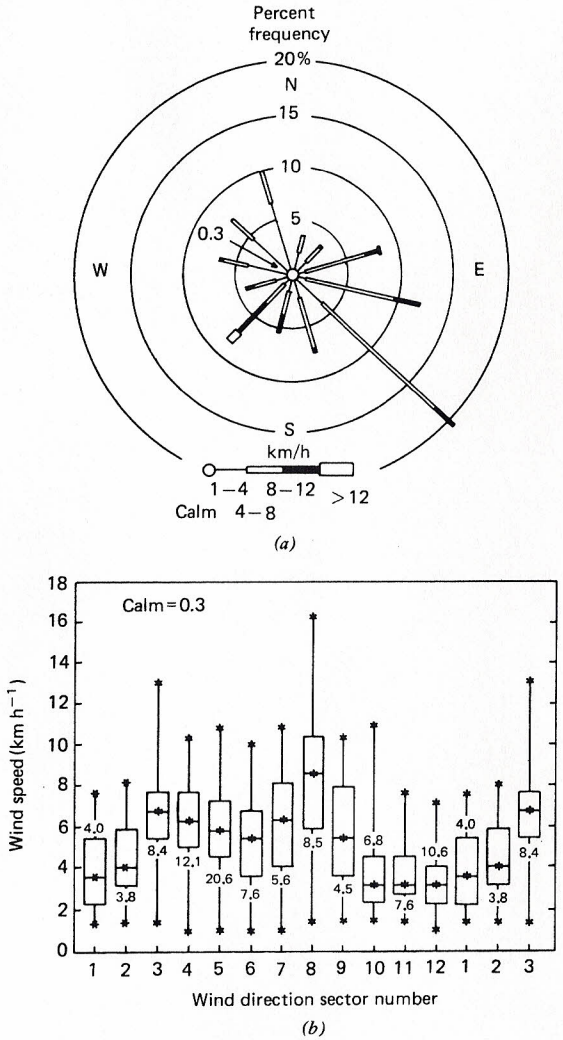

Fig. 4.11 (*a*) Wind rose for hourly averaged wind data, Artesia Junction, New Mexico, August–December 1971. (*b*) Wind box plot for the same data used in (*a*). The upper and lower boundaries of each box indicate the upper and lower quartiles of the distribution; the median value is shown by the asterisk and line within the box; and the extreme upper and lower data values are shown by asterisks above and below the box. Sector centers are 15°, 45°, 75°,. . . . The arbitrary discontinuity at 360° is avoided by duplicate plotting of sectors 1–3. Numbers on the figure refer to the frequency (in percent)) of wind flow within a given sector (adapted from Graedel, 1977).

means of the hourly wind speed recorded over a 14-year period (1948–1961) and were summarized by Rosenberg (1965) on the basis of climatic weeks. Week 1 is March 1–7.

Northwesterly flow dominates the central Great Plains in the early spring, with south to southeasterly flow dominating through late spring and summer. Although in late October the predominant flow is from the northwest, south and southeasterly winds still comprise an important portion of the total.

Graedel (1977) introduced a new method of graphically displaying the distributions of wind speed and direction. This method, called the "wind box plot," displays the characteristics of the distributions clearly and more completely than does the traditional wind rose. Selected characteristics of the distributions, such as the highest value, upper quartile, median, lower quartile and lowest value, are included in a wind box plot. An example taken from Graedel (1977) is shown in Fig. 4.11. This technique is readily adapted to computer statistics and graphics packages.

Figure 4.12 is a representation for the growing season (weeks 1–39) at Grand Island, Nebraska, of the mean day and night horizontal wind speeds (top) and the resultant horizontal wind speeds (bottom) computed for the same data used in Fig. 4.10. The mean day or night horizontal wind speed U_m is simply an average of hourly horizontal wind speeds. The resultant wind speed U_r is calculated by dividing the distance between the original

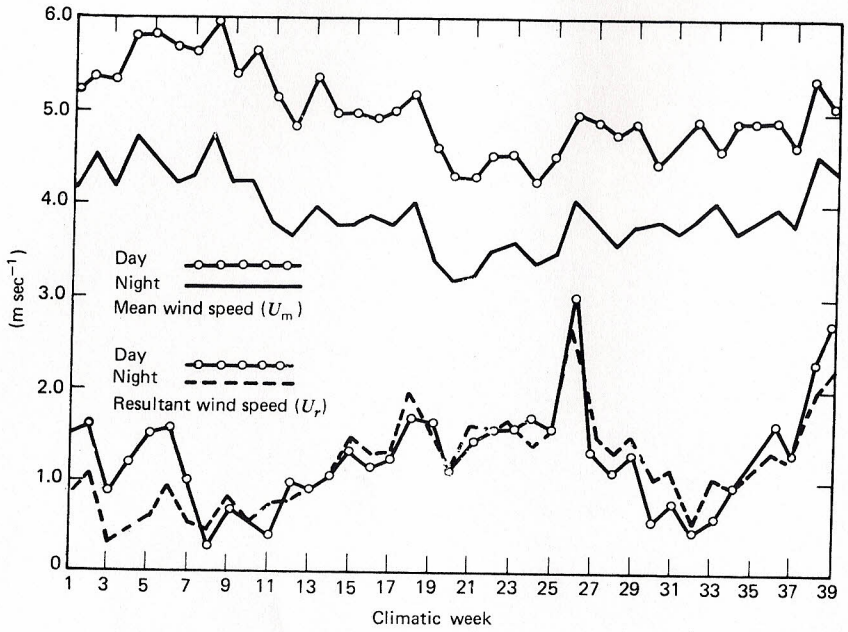

Fig. 4.12 Weekly mean and resultant wind speed at Grand Island, Nebraska (after Rosenberg, 1965).

Table 4.1 Mean and resultant wind speeds and wind directions during the day and night at Grand Island, Nebraska[a]

	Day				Night			
Week	Mean wind speed U_m (m s^{-1})	Resultant wind speed U_r (m s^{-1})	Wind direction (8 pt.)	Constancy C (%)	Mean wind speed U_m (m s^{-1})	Resultant wind speed U_r (m s^{-1})	Wind direction (8 pt.)	Constancy C (%)
01	5.4	1.6	NW	29	4.3	0.8	N	20
02	5.6	1.7	N	30	4.7	1.1	N	24
03	5.5	0.9	N	16	4.3	0.3	NE	7
04	6.0	1.3	NW	21	4.9	0.5	NW	10
05	6.1	1.6	N	26	4.6	0.6	N	13
06	5.9	1.7	N	28	4.4	1.0	N	24
07	5.9	1.0	NE	18	4.5	0.6	W	13
08	6.3	0.3	NE	5	5.0	0.4	SE	9
09	5.6	0.8	SE	14	4.4	0.8	SE	19
10	5.9	0.6	NE	11	4.4	0.6	E	13
11	5.4	0.4	SE	8	3.9	0.8	SE	19
12	5.0	1.0	SE	21	3.8	0.8	SE	21
13	5.6	0.9	SE	16	4.2	0.9	SE	23
14	5.2	1.1	SE	21	3.9	1.1	SE	29
15	5.2	1.4	SE	28	3.9	1.5	SE	39
16	5.1	1.2	S	24	4.0	1.3	SE	34
17	5.2	1.3	S	25	3.9	1.3	SE	34
18	5.4	1.8	S	34	4.2	2.1	SE	50
19	4.8	1.7	S	36	3.5	1.6	SE	46
20	4.5	1.2	SE	26	3.3	1.2	SE	36
21	4.5	1.5	SE	33	3.4	1.7	S	50
22	4.7	1.7	S	35	3.7	1.6	S	46
23	4.7	1.7	SE	36	3.8	1.7	SE	47
24	4.4	1.8	SE	41	3.5	1.4	SE	41
25	4.7	1.7	SE	36	3.6	1.6	SE	46
26	5.2	3.2	S	61	4.3	2.9	S	66
27	5.1	1.4	S	28	3.9	1.7	S	42
28	5.0	1.2	S	23	3.7	1.4	S	37
29	5.1	1.4	S	28	3.9	1.6	S	41
30	4.6	0.6	SW	12	4.0	1.1	S	26
31	4.9	0.8	S	17	3.8	1.2	S	31
32	5.1	0.5	SW	9	4.0	0.6	S	15
33	4.7	0.6	SW	13	4.2	1.1	SW	30
34	5.1	1.0	SW	20	3.8	1.0	S	26
35	5.1	1.3	W	25	4.0	1.2	W	29
36	5.1	1.7	NW	36	4.2	1.4	W	34
37	4.8	1.4	W	29	3.9	1.3	W	33
38	5.6	2.4	NW	43	4.7	2.1	W	43
39	5.2	2.9	NW	56	4.6	2.3	W	51

[a] After Rosenberg (1965).

and final positions of a hypothetical particle of air by the time elapsed in its travel considering the changes in direction that occur.

The constancy C of the wind relates the resultant and mean (day or night) wind speeds by

$$C = \frac{U_r}{U_m} \times 100 \tag{4.27}$$

A constancy of $C = 0$ means a perfectly circular distribution of wind vectors, that is, $U_r = 0$. A constancy of $C = 100$ indicates wind blowing from one direction only, that is, $U_r = U_m$. The techniques of calculating resultant wind speeds and the directions are given by Brooks and Corruthers (1953).

Figure 4.12 and Table 4.1 show that at Grand Island, Nebraska, peak average wind speeds during the growing season occur in the spring with a gradual decrease to midsummer. Whereas wind speeds are lowest in midsummer, they are most constant during that season. Nocturnal average winds are always lower than daytime wind, but the resultant wind speed at night may exceed that during the day. A very sharp increase in constancy occurs during week 26 (August 23–29). After week 32, the constancy of westerly and northwesterly winds increases gradually.

Figures 4.10, 4.11, and 4.12 and Table 4.1 show some alternative ways of representing wind data. The application of the data should determine the methods used. It should be apparent, however, that calculations of mean wind speed and prevailing wind direction when used alone may be of limited value except for very general purposes of climatic description and may, in fact, obscure important relationships.

4.10 WIND SPEED INSTRUMENTATION

A complete discussion of wind sensors is beyond the scope of this work. Those who plan to use wind instruments should refer to authoritative works on meteorological instrumentation to determine the specific type of sensor that best meets the needs and the budget available. Only some general comments on sensor design principles are offered below. The major types of anemometers shown in Fig. 4.13 may be classified as pressure, mechanical, thermoelectric, and acoustical.

The Pitot tube is an example of a pressure anemometer. The difference in pressure developed between two tubes as wind blows into one and transverse to the other is directly related to the wind speed. Pitot tube systems are quite accurate and are usually used as standards for calibrating other types of wind speed sensors. The same principle is used in the anemoclinometer, which measures downwind, crosswind, and vertical components of wind velocity simultaneously. The anemoclinometer (Fig. 4.13*a*) developed by Thurtell et al. (1970) is a small metal sphere with electronic pressure sensors placed in holes facing directly into the wind and at 90° angles to the

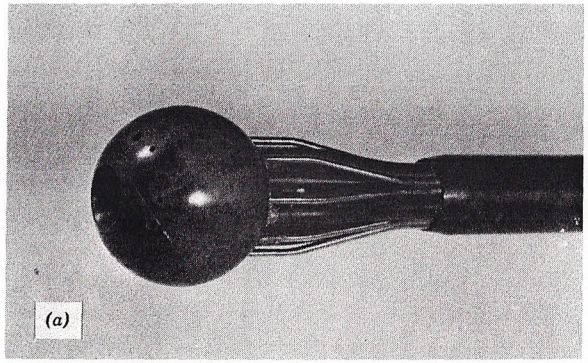

Fig. 4.13 (*a*) Spherical sensing head of the anemoclinometer showing pressure ports (after Thurtell et al., 1970).

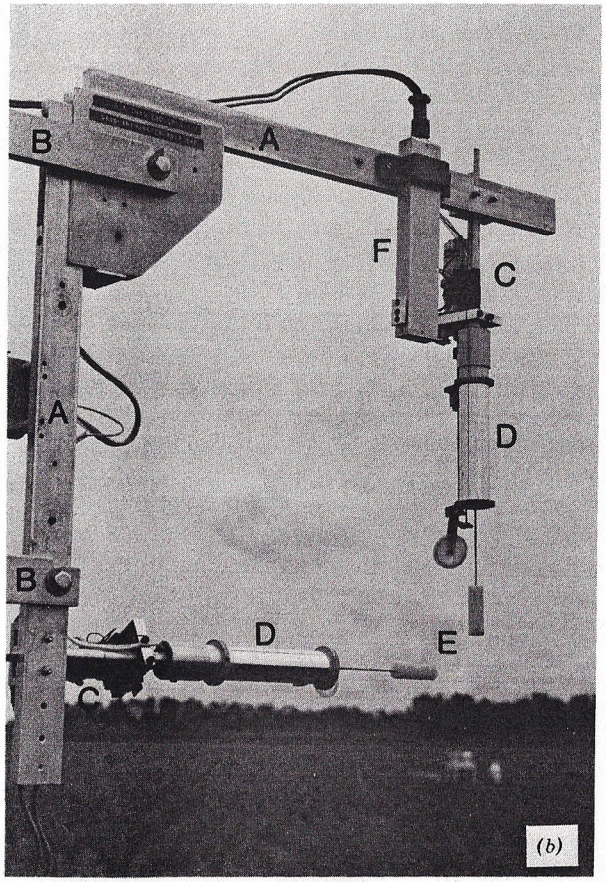

Fig. 4.13 (*b*) Drag anemometer (A, frame; B, mounting brackets; C, shroud motors; D, strain gage assembly housing and shrouds; E, wind sensing elements) and fine wire thermocouple electronics (F) (adapted from Redford et al., 1981).

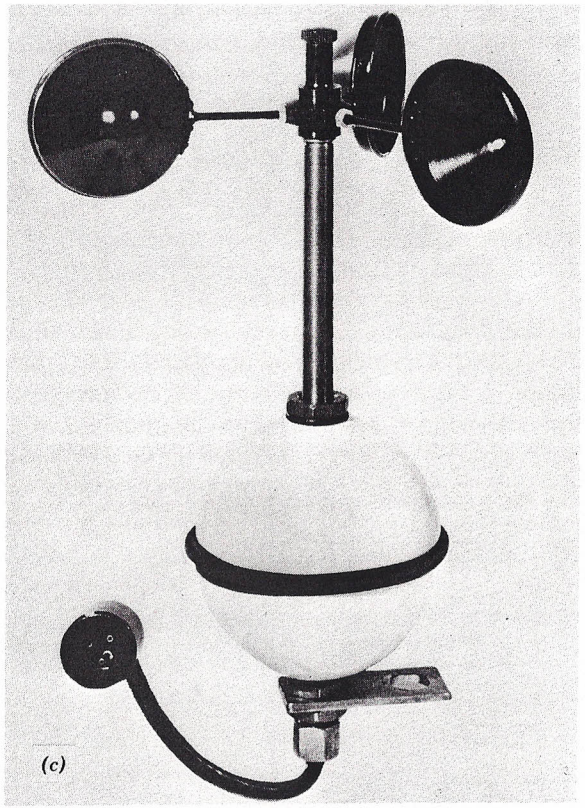

Fig. 4.13 (*c*) Three-cup anemometer (courtesy of Science Associates, Princeton, New Jersey).

main axis. Pressure differences between the various sets of holes are used to calculate the three-dimensional wind speed components.

Rapid fluctuations of wind speed in three dimensions can also be measured with the drag anemometer. The sensor (Fig. 4.13*b*), is described in Norman et al. (1976). Recently Redford et al. (1981) have thoroughly tested the instrument for turbulent flux and spectra measurements over vegetated surfaces. The drag force of the wind on an aerodynamic shape is proportional to the square of the wind speed. This force can be measured by the deflection of a strain gauge attached to an object held perpendicular to the wind. Since the wind is not constant in direction, three mutually perpendicular wind sensing elements with strain gauges attached can be used to resolve the instantaneous wind speed and direction.

Cup anemometers are mechanical devices. One type is shown in Fig. 4.13*c*. The rate of rotation of a cup anemometer is a quadratic function of the mean horizontal wind speed and of certain geometric design parameters

of the cups. Cup anemometers are intended for use in the horizontal position only. The instrument should respond to oblique winds only as the cosine of the attack angle. Cup anemometers start relatively slowly because of their inertia. Cup anemometers tend to "overspeed" primarily due to their non linear response to fluctuating winds. The instrument responds faster to an increase in wind than to a decrease of the same magnitude. Therefore, in gusty winds the mean wind speed measured by a cup anemometer is overestimated, generally by about 10–15%. For further details on the dynamic response of the cup anemometer in fluctuating winds the reader is referred to publications such as Busch and Kristensen (1976) and Wyngaard (1981). Therefore, the smaller the mass of the cups and arms, the better the sensitivity and accuracy. Mechanical contacts or electrical systems (light choppers) are used to record the rotation of the cups. The less the friction and inertia of the internal counting mechanism, the more accurate will be the sensor.

Propeller anemometers have been used to measure air flow. The helicoid-

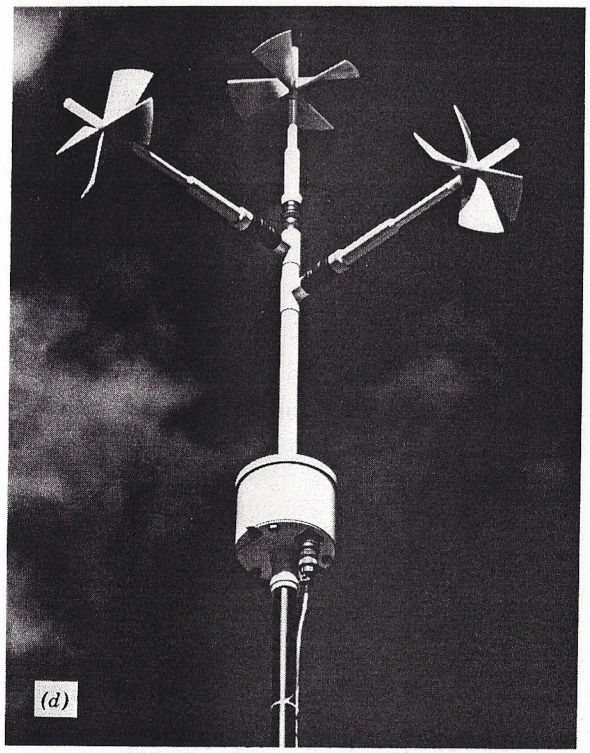

Fig. 4.13 (*d*) UVW propeller anemometer measures directly the three orthogonal wind components (courtesy of R. M. Young Co., Ann Arbor, Michigan).

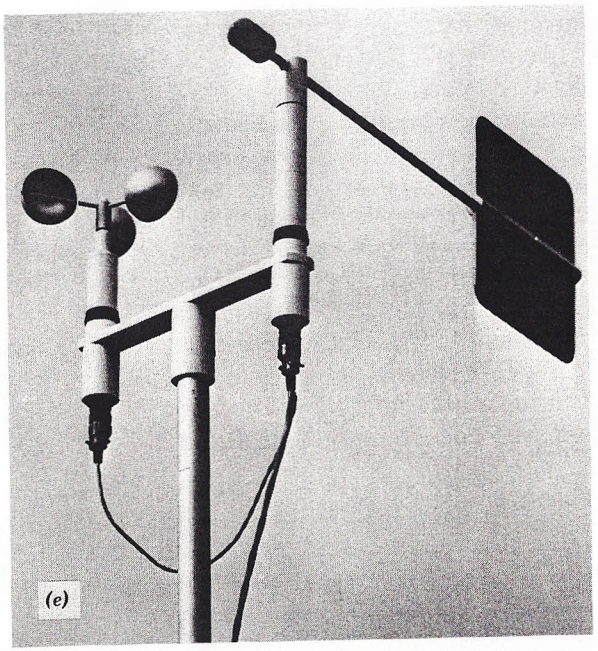

Fig. 4.13 (*e*) The Gill microvane for measuring wind direction, shown with a three-cup anemometer (courtesy of R. M. Young Co., Ann Arbor, Michigan).

shaped polystyrene propeller drives a miniature dc tachometer generator. A propeller responds only to the component of the wind which is parallel to its axis of rotation and thus may be positioned to measure either along wind, across wind, or vertical component of wind velocity. The UVW propeller anemometer system shown in Fig. 4.13*d* consists of three helicoidal propeller sensors mounted on a common mast at right angles to each other and is used to measure the three orthogonal wind components.

Wind vanes available from instrument manufacturers to measure wind direction come in various shapes and sizes. Designs differ primarily in the shape of the fin. One example is shown in Fig. 4.13*e*. A wind vane coupled with a propeller as shown in Fig. 4.13*f*, for example, can be used to measure horizontal wind direction and speed.

Bivanes are employed to obtain simultaneous measurements of azimuth angle and elevation angle of the wind. One type of bivane is shown in Fig. 4.13*g*. A bivane coupled with a propeller, as shown in Fig. 4.13*h*, for example, has been used to measure wind speed plus simultaneous azimuth and elevation angles of the wind.

Thermoelectric anemometry is represented by hot-wire-type sensors. Examples of hot-wire and hot-film anemometers are shown in Fig. 4.13*i*. Anemometers of this kind are particularly useful in applications where wind

speed is very light, as in plant canopies. There are many industrial applications as well where the stream of air or gas is slow and mechanical sensors might interfere with the flow. The rate of convective cooling by a heated body is a function of the rate of fluid flow past that body. One type of hot-wire anemometer is maintained at a constant temperature, while the current flow needed to maintain that temperature is measured. Another type involves constant current flow while temperature fluctuations indicate the fluid flow. Sets of hot wires can be oriented so as to measure the three directional components of wind movement.

Heated thermistor anemometers (Bergen, 1971) have been used for air flow measurements in plant canopies. A heated thermistor anemometer consists of two matched thermistors (see Fig. 4.13*j*). One of the thermistors (A) is exposed to the air movement while the other one (B) is shielded. In still air, the resistances of A and B are equal and there is no voltage drop across the terminals d and f (bottom figure). With some air movement the thermistor

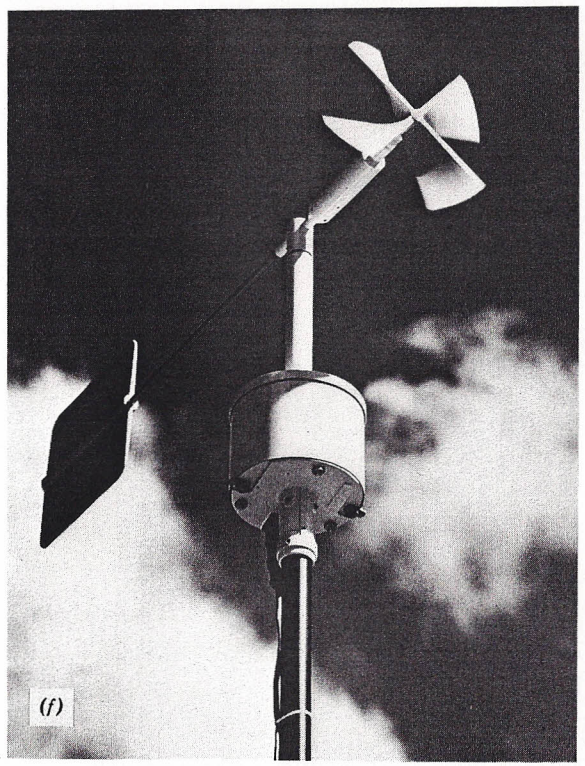

Fig. 4.13 (*f*) Propeller vane for measuring horizontal wind direction and wind speed (courtesy of R. M. Young Co., Ann Arbor, Michigan).

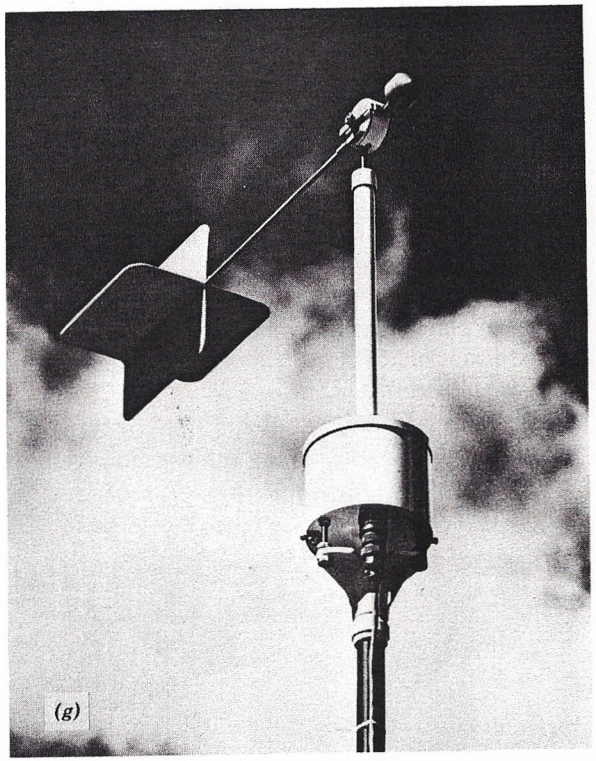

Fig. 4.13 (*g*) Bivane measures the azimuth and elevation angles of the wind (courtesy of R. M. Young Co., Ann Arbor, Michigan).

Fig. 4.13 (*h*) The Gill anemometer bivane measures wind speed plus simultaneous azimuth and elevation angles of the wind (courtesy of R. M. Young Co., Ann Arbor, Michigan).

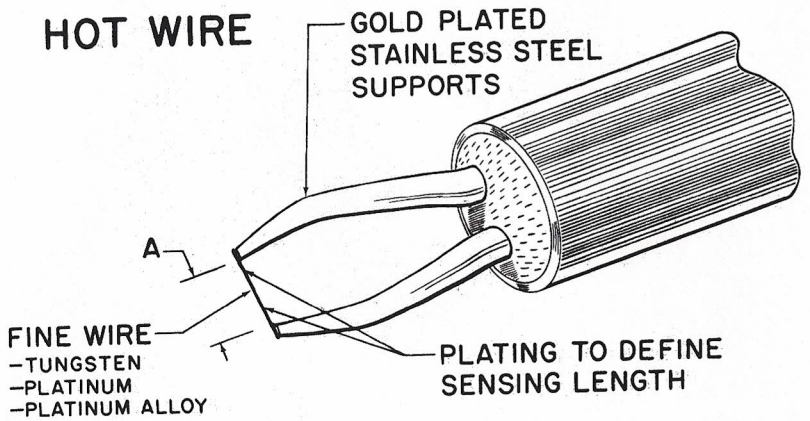

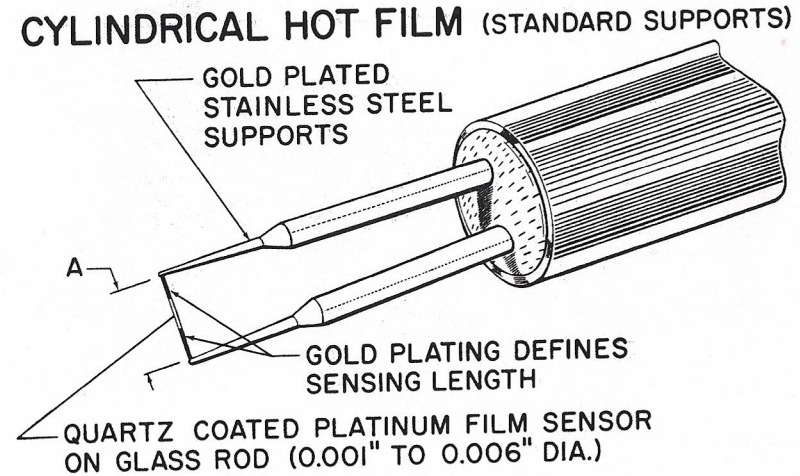

(*i*)

Fig. 4.13 (*i*) Schematic of hot-wire (top) and hot-film (bottom) anemometers (courtesy of Thermo Systems, Inc., St. Paul, Minnesota).

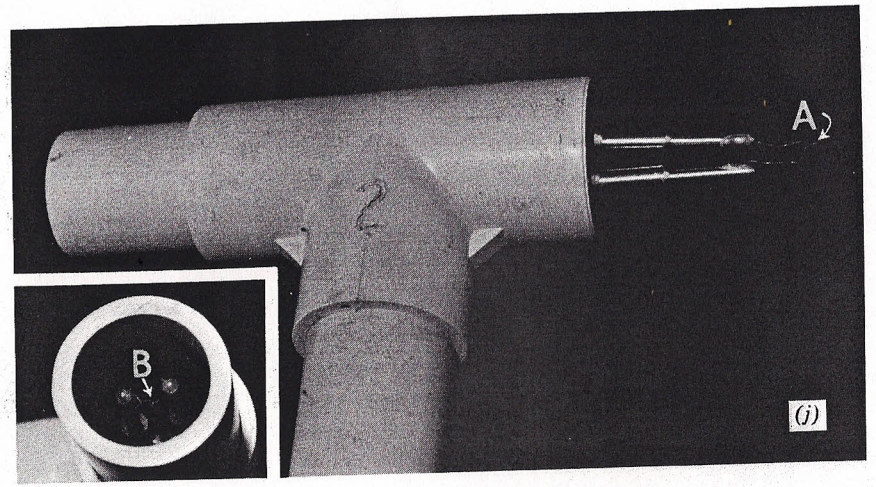

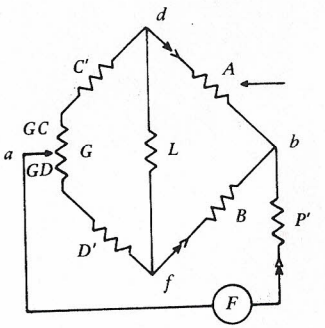

(*j*)

Fig. 4.13 (*j*) Heated thermistor anemometer: (top) a photograph; (bottom) a schematic bridge circuit diagram. A and B are two matched bead thermistors, C' and D' are two fixed resistors, F is a dc voltage source across the bridge, G is a rheostat subdivided into resistances GC and GD, P' represents the equivalent resistance for the connecting cables, and L represents the equivalent resistance of the output meter (adapted from Bergen, 1971; for further explanation see Bergen's paper).

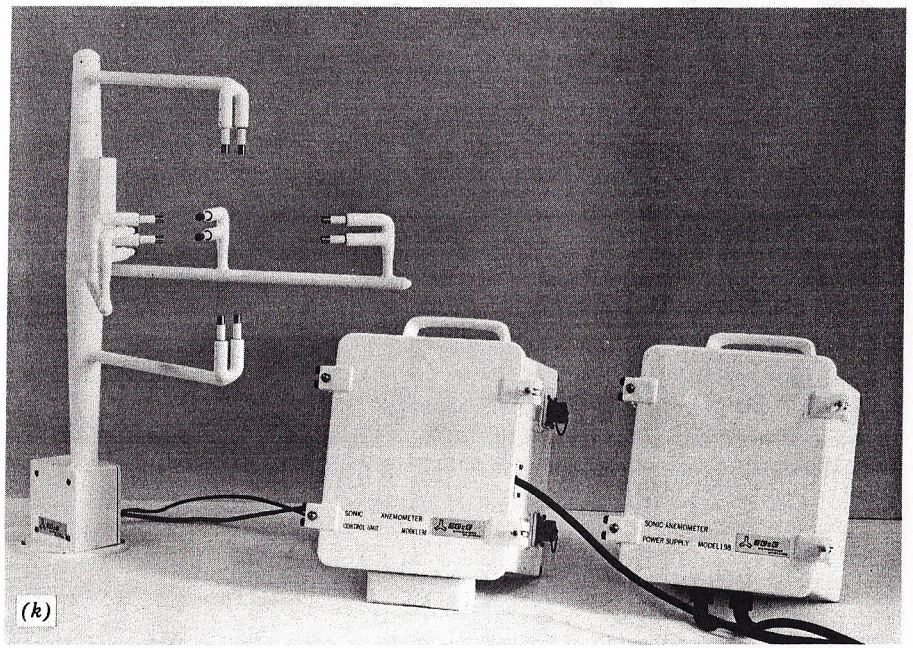

Fig. 4.13 (*k*) Triaxial sonic anemometer (courtesy of EG&G, Cambridge Systems, Inc., Newton, Massachusetts).

A cools and its resistance increases. This change in resistance gives rise to a voltage across points *d* and *f*.

Sonic anemometers are among the newest developments in anemometry. Sound travels faster from an emitter to a receiver in the direction of the wind and, conversely, travels more slowly against the wind. The speed of sound varies with such factors as air temperature, water vapor pressure, and atmospheric pressure. With three sets of emitters and receivers oriented in the *x*, *y*, and *z* directions, it is possible to determine three orthogonal components of wind velocity simultaneously. A three-dimensional sonic anemometer is shown in Fig. 4.13*k*. Campbell and Unsworth (1979) have reported on a one-dimensional (vertical) sonic anemometer. This instrument is relatively inexpensive, and because of the simplicity of its design, appears quite promising.

REFERENCES

Allen, L. H., Jr. 1968. Turbulence and windspeed spectra within a Japanese larch plantation. *J. Appl. Meteorol.* **7**:73–78.

Bergen, J. D. 1971. An inexpensive heated thermistor anemometer. *Agric. Meteorol.* **8**:395–405.

Brooks, C. E. P., and N. Corruthers. 1953. Handbook of Statistical Methods in Meteorology. M.O. 538. Air Ministry, Meteorological Office, H. M. Stationary Office, London.

Busch, N. E., 1973. On the mechanisms of atmospheric turbulence. Workshop on Micrometeorology (D. A. Haugen, ed.). Am. Meteorol. Soc., Boston.

Busch, N. E., and L. Kristensen. 1976. Cup anemometer overspeeding. *J. Appl. Meteorol.* **15**:1328–1332.

Businger, J. A., J. C. Wyngaard, Y. Izumi, and E. F. Bradley. 1971. Flux-profile relationships in the atmospheric surface layer. *J. Atmos. Sci.* **28**:181–189.

Campbell, G. S. 1977. *An Introduction to Environmental Biophysics*. Springer-Verlag, New York. 159 pp.

Campbell, G. S., and M. H. Unsworth. 1979. An inexpensive sonic anemometer for eddy correlation. *J. Appl. Meteorol.* **18**:1072–1077.

Dyer, A. J., and B. B. Hicks. 1970. Flux-gradient relationships in the constant flux layer. *Q. J. Roy. Meteorol. Soc.* **96**:715–721.

Dyer, A. J. 1974. A review of flux-profile relationships. *Boundary-Layer Meteorol.* **7**:363–372.

Francey, R. J., and J. R. Garratt. 1981. Interpretation of flux-profile observations at ITCE (1976). *J. Appl. Meteorol.* **20**:603–618.

Garratt, J. R. 1980. Surface influence upon vertical profiles in the atmospheric near-surface layer. *Q. J. Roy. Meteorol. Soc.* **106**:803–819.

Graedel, T. E. 1977. The wind box plot: An improved wind rose. *J. Appl. Meteorol.* **16**:448–450.

Holzman, B. 1943. The influence of stability on evaporation. *Ann. N.Y. Acad. Sci.* **44**:13–18.

Kanemasu, E. T., M. L. Wesely, B. B. Hicks, and J. L. Heilman. 1979. Techniques for calculating energy and mass fluxes. *Modification of the Aerial Environment of Crops* (B. J. Barfield and J. F. Gerber, eds.). Am. Soc. Agric. Engineers, St. Joseph, Michigan.

Lemon, E. 1969. Gaseous exchange in crop stands. *Physiological Aspects of Crop Yield* (J. D. Eastin, F. A. Haskins, C. Y. Sullivan, and C. H. M. van Bavel, eds.). Am. Soc. of Agronomy, Madison, Wisconsin.

Lumley, J. L., and H. A. Panofsky. 1964. *The Structure of Atmospheric Turbulence*. Wiley, New York. 239 pp.

Makkink, G. F., and H. D. J. van Heemst. 1970. *Potential Evaporation from a Canopy*. Institute for Biological and Chemical Research on Crops, Wageningen, Meded. 417. In Dutch (English summary).

Monin, A. S., and A. M. Obukhov. 1954. The basic laws of turbulent mixing in the surface layer of the atmosphere. *Akad. Nauk USSR Acad. Sci.* **24**:163–187.

Monteith, J. L. 1973. *Principles of Environmental Physics*. Edward Arnold, London. 241 pp.

Munro, D. S., and T. R. Oke. 1975. Aerodynamic boundary-layer adjustment over a crop in neutral stability. *Boundary-Layer Meteorol.* **9**:53–61.

Norman, J. M., S. G. Perry, and H. A. Panofsky. 1976. Measurement of theory of horizontal coherence at a two-meter height. Preprints, Third Symposium on Atmospheric Turbulence, Diffusion and Air Quality, American Meteorological Society, October 19–22, 1976, Raleigh, North Carolina, pp. 26–31.

Oke, T. R. 1970. Turbulent transport near the ground in stable conditions. *J. Appl. Meteorol.* **9**:778–786.

Oke, T. R. 1978. *Boundary Layer Climates*. Methuen and Co. Ltd., London. 372 pp.

Panofsky, H. A. 1963. Determination of stress from wind and temperature measurements. *Q. J. Roy. Meteorol. Soc.* **89**:85–94.

Plate, E. J. 1971. Aerodynamic Characteristics of Atmospheric Boundary Layer. U.S. Atomic Energy Commission. NTIS TID-25465, 190 pp.

Pruitt, W. O., D. L. Morgan, and F. J. Lourence. 1973. Momentum and mass transfer in the surface boundary layer. *Q. J. Roy. Meteorol. Soc.* **99**:370–386.

Redford, Jr., T. G., S. B. Verma, and N. J. Rosenberg. 1981. Drag anemometer measurements of turbulence over a vegetated surface. *J. Appl. Meteorol.* **20**:1222–1230.

Rosenberg, N. J. 1965. Climate of the central Platte Valley of Nebraska. *Nebr. Agric Exp. Stn. Misc. Bull.* **11**, part B.

Slade, D. H., ed. 1968. Meteorology and Atomic Energy. U.S. Atomic Energy Commission, Office of Information Services. 445 pp.

Stanhill, G. 1969. A simple instrument for field measurement of turbulent diffusion flux. *J. Appl. Meteorol.* **8**:509–513.

Sutton, O. G. 1953. *Micrometeorology*. McGraw-Hill, New York. 333 pp.

Swinbank, W. C. 1964. The exponential wind profile. *Q. J. Roy. Meteorol. Soc.* **90**:119–135.

Swinbank, W. C. 1968. A comparison between predictions of dimensional analysis for the constant-flux layer and observations in unstable conditions. *Q. J. Roy. Meteorol. Soc.* **94**:460–467.

Szeicz, G., G. Endrodi, and S. Tajchman. 1969. Aerodynamic and surface factors in evaporation. *Water Resour. Res.* **5**:380–394.

Thom, A. S. 1971. Momentum absorption by vegetation. *Q. J. Roy. Meteorol. Soc.* **97**:414–418.

Thom, A. S. 1975. Momentum, mass and heat exchange of plant communities. *Vegetation and the Atmosphere* (J.. L. Monteith, ed.), Academic Press, pp. 57–109.

Thurtell, G. W., C. B. Tanner, and M. L. Wesely. 1970. Three-dimensional pressure sphere anemometer system. *J. Appl. Meteorol.* **9**:379–385.

Webb, E. K. 1965. *Aerial Microclimate*. Meteorological Monographs. Vol. 6, No. 28, Chapter 2, pp. 27–58.

Webb, E. K. 1970. Profile relationships: The log-linear range, and extension to strong stability. *Q. J. Roy. Meteorol. Soc.* **96**:67–90.

Webb, E. K., G. I. Pearman, and R. Leuning. 1980. Correction of flux measurements for density effects due to heat and water vapour transfer. *Q. J. Roy. Meteorol. Soc.* **106**:85–100.

Webb, E. K. 1982. On the correction of flux measurements for effects of heat and water vapour transfer. *Boundary-Layer Meteorol.* **23**:251–254.

Wieringa, J. 1980. A revaluation of the Kansas mast influence on measurements of stress and cup anemometer overspeeding. *Boundary-Layer Meteorol.* **18**:411–430.

Wyngaard, J. C. 1981. Cup, propeller, vane and sonic anemometers in turbulence research. *Annu. Rev. Fluid Mech.* **13**:399–423.